JOURNAL OF CATALYSIS 70, 308–322 (1981)

Physical Characterization of Fe/TiO_2 Model Supported Catalysts

I. Electron Microscopic Studies of Reduction Behavior

B. J. TATARCHUK[1] AND J. A. DUMESIC[2]

Department of Chemical Engineering, University of Wisconsin, Madison, Wisconsin 53706

Received December 2, 1980; revised April 3, 1981

The morphology of Fe/TiO_2 model supported catalysts has been monitored using transmission electron microscopy following hydrogen reduction at progressively higher temperatures. Nucleation and growth of iron particles from an initially contiguous iron overlayer was observed in the temperature range 608 to 707 K. Following reduction at 773 K, the smaller iron crystallites (less than 10 nm in size) were observed to spread over or wet the support surface, and reduction at temperatures of 875 K or higher extended this spreading behavior to larger crystallites. In addition, reduction at these latter temperatures caused decreases in the average iron particle size and the amount of iron present on the support as distinct iron crystallites. This can be attributed to a diffuse spreading of iron *over* the support or a diffusion of iron *into* the support.

INTRODUCTION

The interactions between metal and support in supported metal catalysts are of current academic and industrial interest. Of particular importance for the present study was the observation by workers at Exxon of "strong metal–support interactions (SMSI)" for Group VIII metals supported on such materials as TiO_2 (*1–4*). This interaction was manifested by the suppression of carbon monoxide and molecular hydrogen chemisorption following high-temperature (ca. 773 K) reduction of these supported metal catalysts. Characterization of these systems using electron microscopy and X-ray diffraction showed that this loss of chemisorption after high-temperature reduction was not the result of metal sintering. Moreover, high-resolution electron microscopic studies of the Pt/TiO_2 system (*3, 4*) indicated that the Pt crystallites assumed a "pillbox" (or thin-raft) morphology following high-temperature H_2 reduction. This was believed to result from the strong Pt/TiO_2 interaction as was the concomitant reduction of the support to Ti_4O_7. Furthermore, this reduction of the support was seen to be catalyzed by Pt. That the strong metal–support interaction is, in fact, related to the reduction of the support was suggested by the observation of similar support interactions for Ir on other reducible supports such as Nb_2O_5, V_2O_3, and Ta_2O_5 (*2*).

Titania-supported systems which show strong metal–support interactions, as characterized by chemisorptive methods, currently include supported Ni, Ru, Rh, Pd, Os, Ir, and Pt. Some of these systems also possess interesting catalytic properties. For example, Ni/TiO_2 (*5*), Ru/TiO_2 (*6*), and Rh/TiO_2 (*7*) appear to be promising catalysts for CO/H_2 synthesis reactions. The Ni/TiO_2 system had higher activity, promoted longer chain growth, produced less $Ni(CO)_4$, and showed less catalyst deactivation than either bulk nickel or nickel on other supports. Ru/TiO_2 produced more olefins and correspondingly less methane as compared to other Ru catalysts. The

[1] Present address: Department of Chemical Engineering, Auburn University, Auburn, Alabama 36849.

[2] To whom correspondence should be addressed; Camille and Henry Dreyfus Foundation Teacher-Scholar.

0021-9517/81/080308-15$02.00/0

Rh/TiO_2 system, when compared to Rh/Al_2O_3, was found to have a higher CO hydrogenation activity and produced significant amounts of alcohols, which increased with increasing reactant pressures (*7*). In other kinetic studies (*8*), Rh/TiO_2 and Pt/TiO_2 catalysts showed marked decreases in their benzene hydrogenation and cyclohexane dehydrogenation activities following high-temperature reduction (ca. 723 K).

While the existence of strong metal–support interactions has been related to the reducibility of the support, the nature of the chemical bonding between metal and support is still a subject of current research effort. Tauster and co-workers (*1*), following their initial chemisorption experiments, suggested that the metal–support interaction involves either bonding between cations of titanium and the noble metals as in the hexagonal barium titanates (*9*) or metallic bonding as in the case of intermetallics. In any case, the existence of titanium in an oxidation state lower than Ti^{4+} was deemed necessary for the presence of strong metal–support interactions. Reduction of the support was also a key concept in the work of Baker *et al.* (*3, 4*) who suggested that the formation of bonds between Pt and Ti^{3+} may be the origin of the observed SMSI effects. Indeed, the possibility of such bonding was supported by the efforts of Horsley (*10*), who conducted an x-alpha scattered wave calculation on the Pt/TiO_2–H_2 system. Vannice and Garten (*6*), in discussing CO hydrogenation over Ru/TiO_2, suggested that high-temperature reduction may increase the concentration of electron acceptor defect sites on the TiO_2 surface (*11*). These sites would then interact with the supported crystallites to decrease the concentration of *d*-band electrons in the metal. In other studies (*8*), electrical conductivity measurements of Pt/TiO_2 and Rh/TiO_2 catalysts have shown that these solids behave as *n*-type semiconductors, the conductivity of which increases with increasing temperature of reduction. Subsequent kinetic measurements were then interpreted in terms of an adjustment of the Fermi levels between the metal and semiconductor support.

In view of the difficulty in characterizing the nature of metal–support interactions in real catalytic materials (i.e., high-surface-area powders), the rationale of the present study was to use "model supported catalysts." As a definition, a model supported catalyst consists of a thin oxide film (i.e., the support) onto which the catalytically active metal has been deposited. Such materials are ideally suited for characterization by transmission electron microscopy (TEM) and X-ray photoelectron spectroscopy (XPS). The "model system" chosen to study strong metal–support interactions was Fe/TiO_2. This was done to permit the use of conversion electron Mössbauer spectroscopy (CEMS) to monitor changes in the chemical state of iron, induced by interactions with TiO_2. In short, the study of Fe/TiO_2 model supported catalysts enables collection of detailed structural and morphological information from both the support and metal phases using TEM, determination of the metal/support electronic and chemical properties using XPS, and detailed electronic, morphological, and magnetic characterization of the iron phase using CEMS.

For clarity, the present work is divided into three contiguous papers. Part I involves the transmission electron microscopic results obtained from Fe/TiO_2 systems, following reduction treatments at progressively higher temperatures; Part II deals with electron spectroscopic (XPS, CEMS) characterization of Fe/TiO_2 model supported catalysts following these same reduction treatments, and Part III considers the reversibility of these reduction trends following oxidation treatments, as studied by electron microscopic and spectroscopic techniques (TEM, XPS, CEMS). Finally, the results from these different studies are summarized in Part III, and an overall discussion of the Fe/TiO_2 system behavior is presented.

EXPERIMENTAL

Sample Preparation

High-purity titanium foils (Alfa-Ventron 99.7%), approximately 60 × 60 × 0.0125 mm, were chemically cleaned in successive solutions of trichloroethylene, acetone, methanol, and distilled–deionized water, respectively. Chemical etching, or smoothing, was then carried out for approximately 30 s using an aqueous solution of 10% nitric and 2% hydrofluoric acids (see Fig. 1). Foils so treated were then oxidized for 2 to 3 h at 570–670 K in oxygen (101 kPa, 99.6% purity, containing 31 ppm trace hydrocarbons). This treatment produces primarily rutile TiO_2 overlayers (*12–14*) on the order of ~50 nm thick. Following this treatment, the oxidized foil was cut into three distinct segments. The metal backing of one segment was then dissolved away using a more diluted form of the original etching solution. Specifically, the etchant solution was added dropwise to a beaker containing H_2O and the oxidized foil until small bubbles appeared at the metal edges. At this concentration the remaining metal foil dissolved in approximately 1 h, leaving the oxide film floating on the surface of the aqueous solution. This film was stable on this solution for indefinite periods of time. Once floated, these oxide films were rinsed in methanol and water and placed on standard 3-mm tungsten or titanium electron microscopy grids (Pelco).

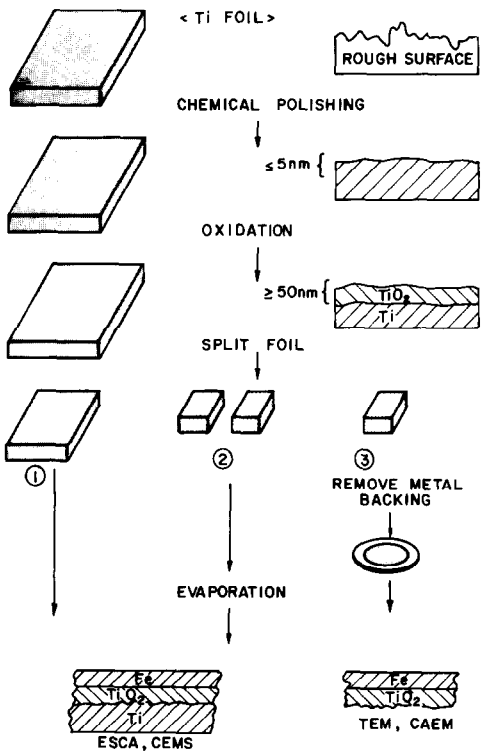

FIG. 1. Schematic of sample preparation.

All three foil segments (see Fig. 1) were then placed in a vacuum metal-evaporator, and simultaneously coated with approximately 2.5 to 5 nm of iron, depending on the loading desired. Small solid angles were employed during this procedure to ensure better than 95% uniformity in iron thickness over all such samples. Before evaporation, the iron (enriched to 91% ^{57}Fe, Oak Ridge) was reduced at 1070 K in flowing hydrogen (101 kPa, 99.999%) for 2 h and placed in a preflashed alumina-coated moly-dimple boat (R. D. Mathis). Iron evaporation onto TiO_2 was subsequently carried out at background pressures of approximately 1.3×10^{-5} Pa. XPS and Auger electron spectroscopy (AES) demonstrated that iron was the only metal deposited on the sample during this procedure (e.g., no Mo was deposited). In addition, approximately two monolayers equivalent of carbon contamination was present on the samples following metal deposition and removal from the coating chamber. The amount of iron deposited was estimated in a number of ways. These included (i) TEM contrast (mass) balances following nucleation of the overlayer into three-dimensional crystallites. (ii) CEMS spectral area measurements, (iii) Fe/Ti spectral intensity ratios measured by XPS, (iv) d.c. sputtering times using a calibrated Ar beam in conjunction with XPS, and (v) the use of a quartz crystal thickness monitor, calibrated employing fixed solid angles and evaporation of measured amounts of iron. By using

these techniques it was possible to estimate the initial iron overlayer thicknesses with an accuracy of about 20% in the range from 2.5 to 5 nm.

In summary, three distinct sets of samples were prepared, as described above. This is shown schematically in Fig. 1. Iron supported on TiO_2 films, from which the Ti metal backing had been previously removed, were used for TEM and controlled-atmosphere electron microscopy (CAEM), since these samples are thin and transparent to an electron beam. The results of TEM are presented in this paper, while the results of CAEM are presented elsewhere (*15*). Samples consisting of iron supported on TiO_2 films, which retained the Ti metal backing, were used for XPS and CEMS experiments, as the thick metal backing served as a structural support for the larger sample areas needed (ca. 1 × 1 cm and 5 × 5 cm, respectively).

Sample Treatment

In order to preserve the analogous nature of the sample preparations for the TEM, XPS, and CEMS studies, fixed temperature schedules and gaseous treatment conditions were employed in all studies. These are given in Table 1. Furthermore, the hydrogen pressure (ca. 10^{-2} Pa) and the H_2/H_2O ratio (ca. 100) during the various TEM and XPS reduction treatments were held constant for all studies. This was accomplished by treating the samples for TEM in the "reaction chamber" of the apparatus used for the XPS studies, the details of which are shown in Part II of this series.

TABLE 1

Sample Treatment Conditions[a]

Reduction temperature[b] (K)	Reduction time (h)
Initial iron overlayer	—
608	4.5
643	3.8
677	3.0
707	3.0
773	3.0
875	3.0
928	3.0

[a] Reduction treatments at $P_{H_2}/P_{H_2O} \cong 100$; total pressure $\cong 1.33 \times 10^{-2}$ Pa.

[b] Temperature maintained within 0.5%.

For completeness, it should be noted that the treatment of samples for TEM differed from that for XPS or CEMS (or CAEM) in one subtle way: the samples for TEM had to be removed from the hydrogen treatment chamber (and thereby exposed to air) prior to analysis in the electron microscope. In addition, after the TEM study, some samples were returned to the hydrogen reduction chamber for further treatment. For the XPS and CEMS studies, however, the various reduction treatments were performed sequentially on the same sample with only exposure to the background vacuum between treatments or during analysis. Thus, three different sets of TEM experiments were performed. One set consisted of the stepwise heating of the *same* sample to progressively higher reduction temperatures, with TEM analysis between each treatment. The second set of experiments involved specimens that had been treated just once, each at a different reduction temperature. And the third set involved specimens that were treated according to the appropriate reaction schedule, with exposure to air and TEM analysis permitted only after completion of a fixed number of sequential reduction steps. Within experimental error, these three sets of experiments gave equivalent results. Thus, while the results reported here are primarily for samples that have undergone progressively higher temperature reduction with exposure to air following the final treatment, it can be concluded that the temperature of the final reduction is more important than the reduction sequence in dictating the structure of the catalyst. This facilitates the comparison of results from TEM with those from XPS and CEMS.

Transmission Electron Microscopy

Analysis was performed using an AEI 802 transmission electron microscope which when operated at 80 kV beam energy had a working resolution of approximately 1.5 nm. Background pressures were better than 1×10^{-3} Pa. Magnification settings were calibrated against standard carbon gratings (Pelco).

RESULTS/DISCUSSION

Iron-Free Support Films

Figure 2A shows an electron micrograph of an iron-free TiO_2 film, floated according to the previously discussed procedures. Transmitted electron diffraction showed the film to be polycrystalline, with little or no change in structure (or diffraction pattern) following heating to 973 K in oxygen. Treatment in hydrogen at 973 K, however, was seen to affect the morphology of these films, as shown in Fig. 2B. Thus, the restructuring or sintering shown in Fig. 2B seems to be related to the presence of hydrogen with possibly some surface reduction of the titania support. This process

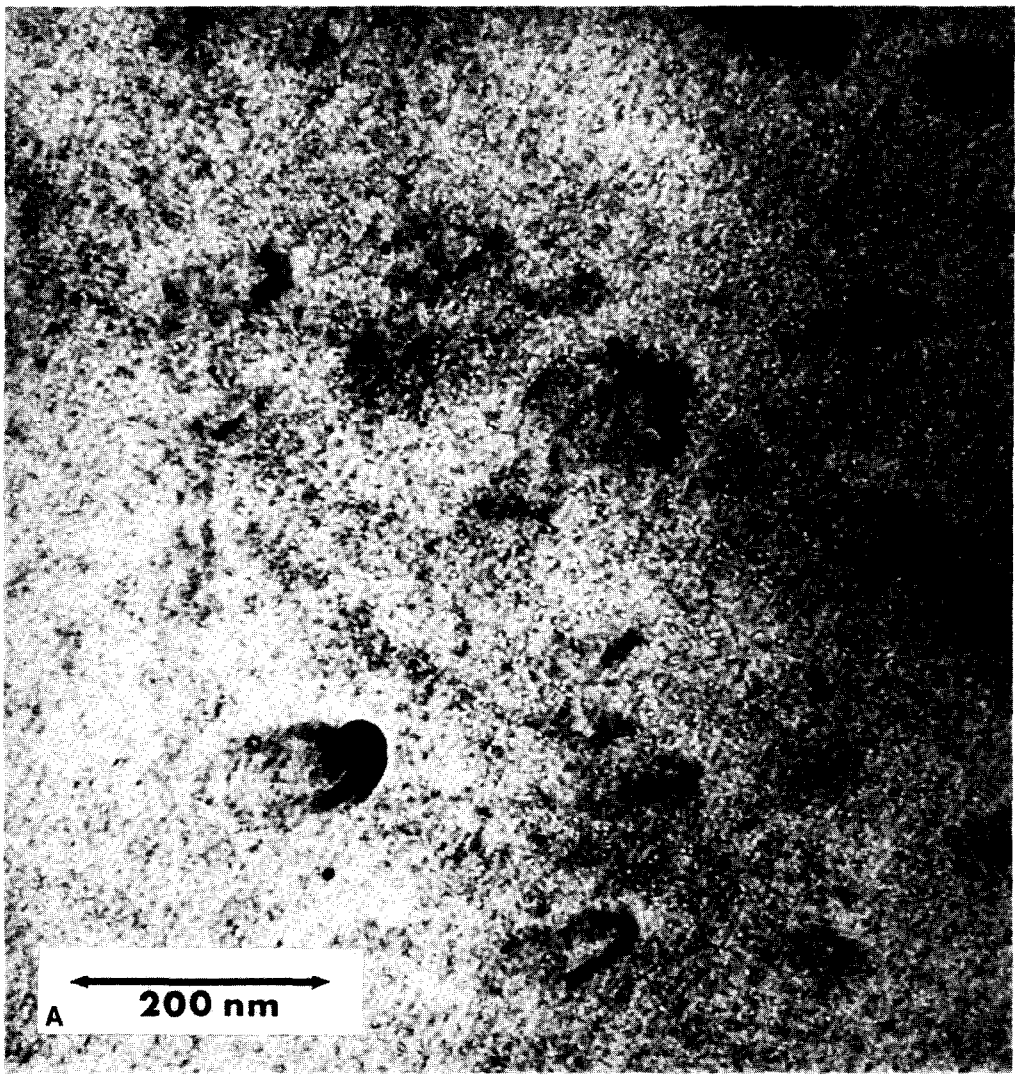

FIG. 2A. TiO_2 film as floated.

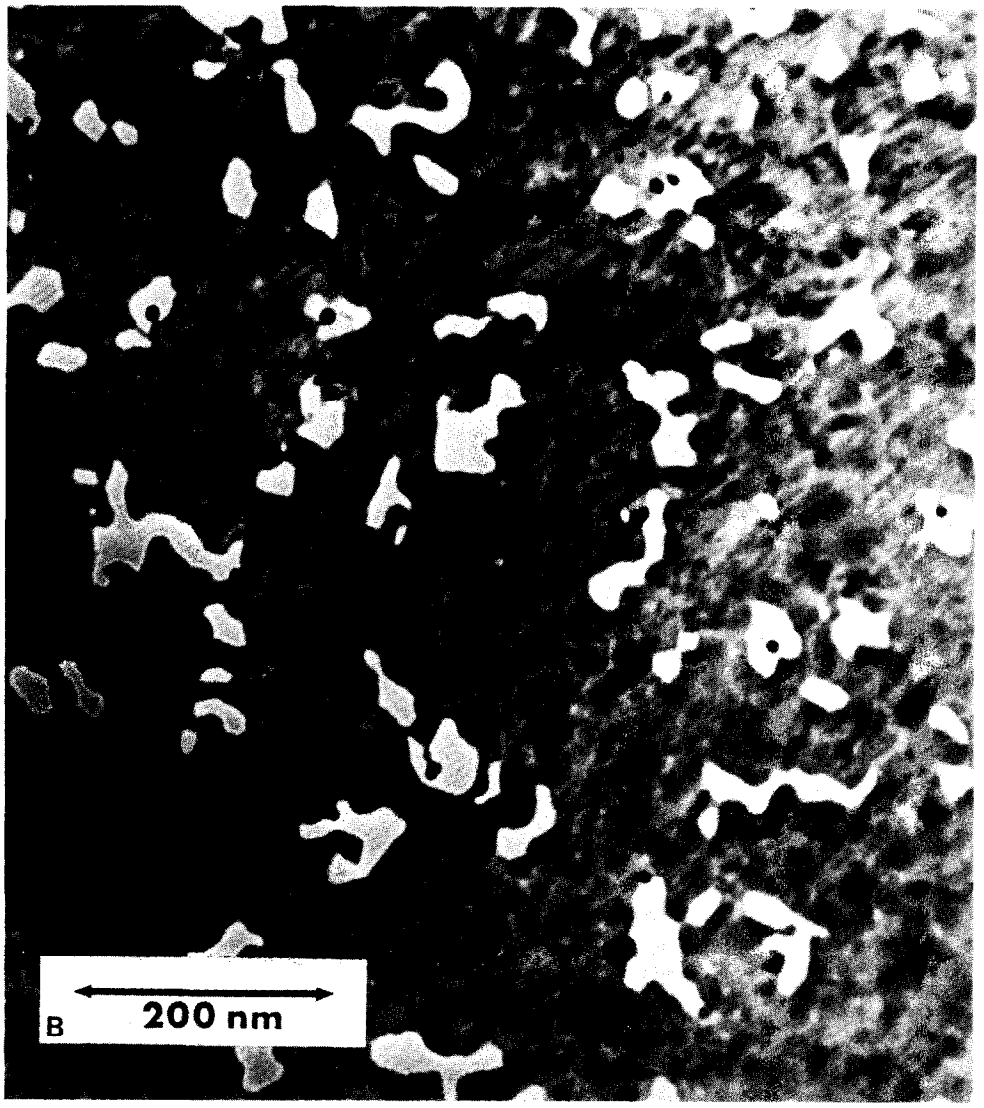

FIG. 2B. TiO_2 film following hydrogen reduction at 973 K for 3 h.

results in the formation of a number of small yet highly contrasted regions. Indeed, the partial reduction of TiO_2 under similar conditions has been reported in the literature (*16–20*).

Iron Overlayer prior to Reduction

Two sets of samples were prepared, with average iron overlayer thicknesses of approximately 3.8 and 5.0 nm, respectively. For brevity, only the series of samples with the 5-nm iron overlayer will be followed in detail. Unless otherwise stated, the reduction behavior of the 3.8-nm Fe specimens was equivalent to that of the 5-nm samples.

Figure 2C shows a TiO_2 film, such as that of Fig. 2A, which had subsequently been coated with 5.0 nm of Fe. During this iron evaporation procedure, the TiO_2 substrates were located far from the hot iron source (20–25 cm) and affixed to a sample holder at room temperature and of high heat capacity. By minimizing sample heating during evaporation, a "contiguous" iron overlayer

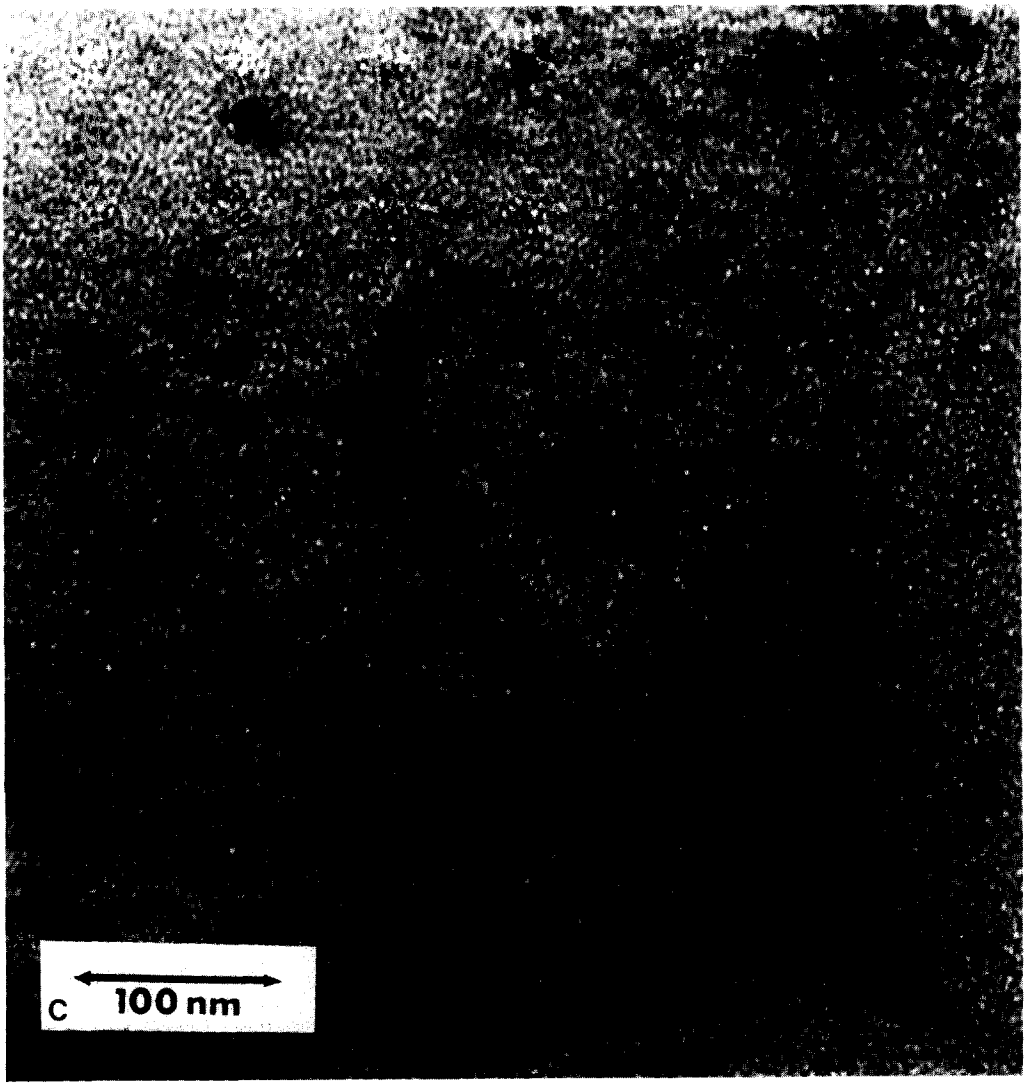

FIG. 2C. Initial Fe/TiO_2 specimen prepared by depositing 5-nm Fe overlayer on TiO_2.

(as opposed to discrete iron particles) is favored. Indeed, within the resolution limit of the microscope (ca. 1.5 nm), nucleation of the iron into separate crystallites did not occur during this sample preparation procedure. Samples of this type constituted the starting point for subsequent reduction experiments.

Reduction at Temperatures of 707 K *or Lower*

Reduction of specimens at 608 and 643 K (see Table 1) led to nucleation at a number of isolated regions on the TiO_2 film. One of these regions is shown in Fig. 3, following reduction at 643 K. The micrograph of Fig. 3 is nearly identical to those taken following reduction at 608 K, except that the higher reduction temperature (643 K) increases the number and size of these nucleated regions. The origin of this nonuniform nucleation is not well understood. It was observed, however, that nucleation of the iron overlayer into crystallites took place preferentially at rough (or structured) support regions, possibly indicating that

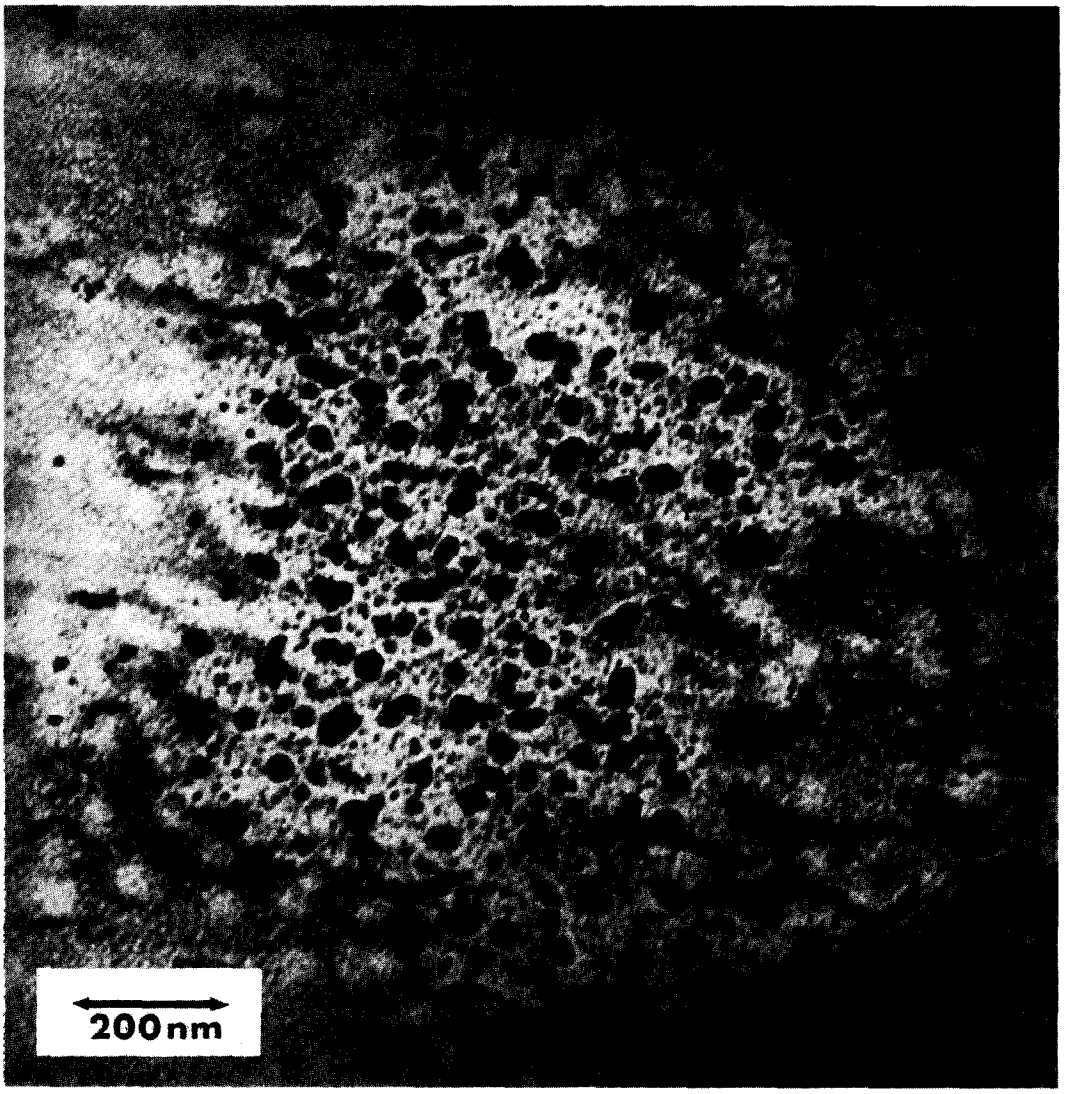

FIG. 3. A 5-nm Fe/TiO_2 specimen following reduction at 643 K for 3.8 h (see Table 1).

reduction/nucleation occurred more readily at these sites. Nevertheless subsequent reduction at higher temperatures (677 and 707 K, Table 1) resulted in uniform nucleation across the surface of the support, following which the location of initial nucleation regions was indiscernible. Figure 4 is an electron micrograph taken after reduction at 707 K. Except for slight changes in particle size, Fig. 4 is nearly identical to micrographs taken after reduction at 677 K, at which point complete nucleation was in all cases observed. It should be noted that extended microscopic analyses at either of these conditions led to observable amounts of carbon contamination at crystallite locations (i.e., dark halos surrounding the iron particles). Neglecting the presence of these halos does not alter interpretation of these micrographs. That is, iron particles formed following reduction at 677 and 707 K are highly contrasted (appear to be dark) compared to the surrounding support phase. Furthermore this

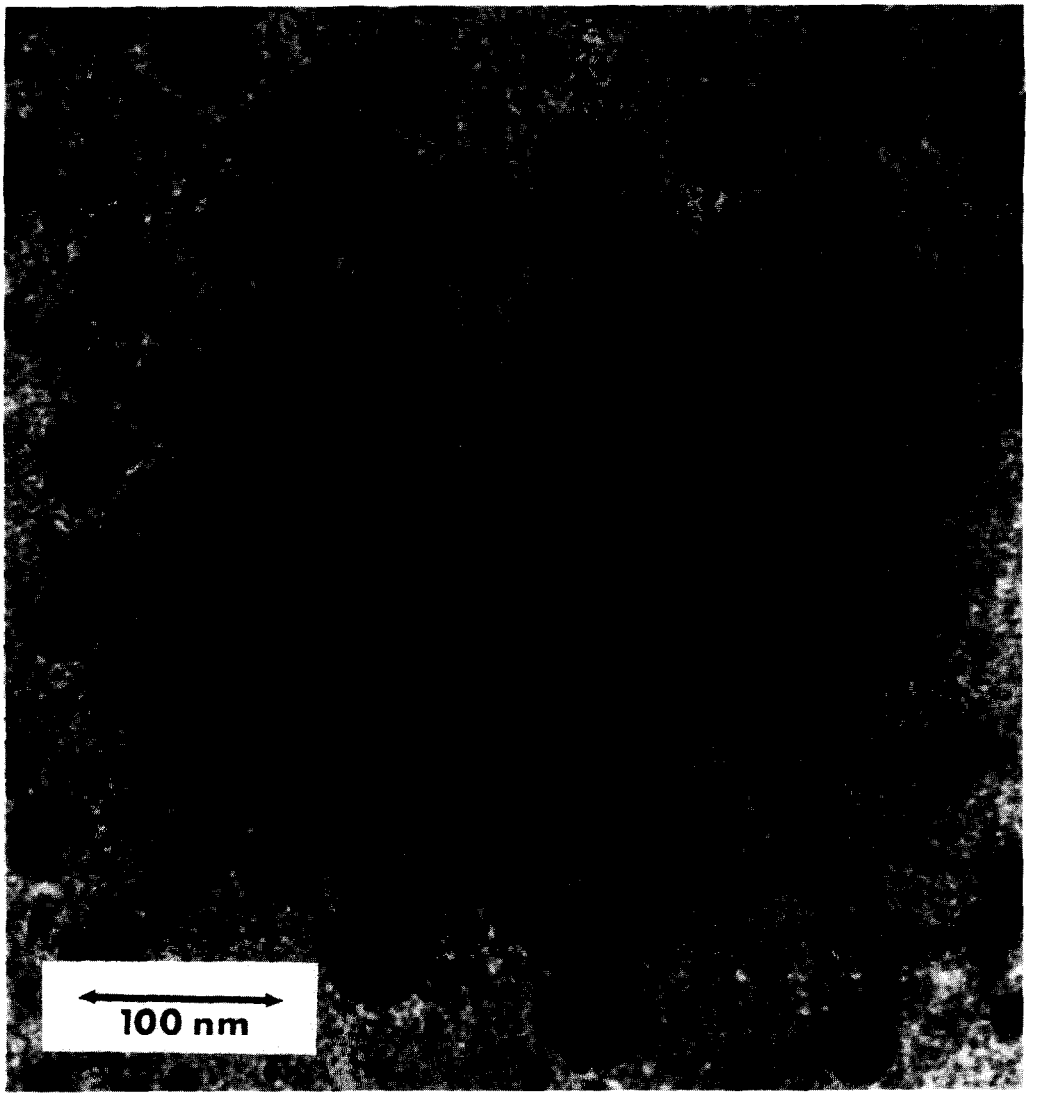

FIG. 4. A 5-nm Fe/TiO_2 specimen following reduction at 707 K for 3 h (see Table 1).

contrast difference is observed for essentially all of the iron crystallites, including those at the smaller end of the particle size distribution. This is interpreted as indicating that iron crystallites reduced at these conditions, regardless of size, assume a three-dimensional morphology on the support surface.

Reduction at 773 K

Figure 5 is an electron micrograph taken after reduction at 773 K (Table 1). Of importance is the observation that many of the smaller iron crystallites show low contrast (appear to be light) compared to the support. Additionally, a few of the larger particles have this low-contrast appearance as well, although this phenomenon occurs predominantly among the smaller crystallites. The presence of adjacent particles possessing approximately equal diameters and yet markedly different contrasts is unmistakable after reduction at this tempera-

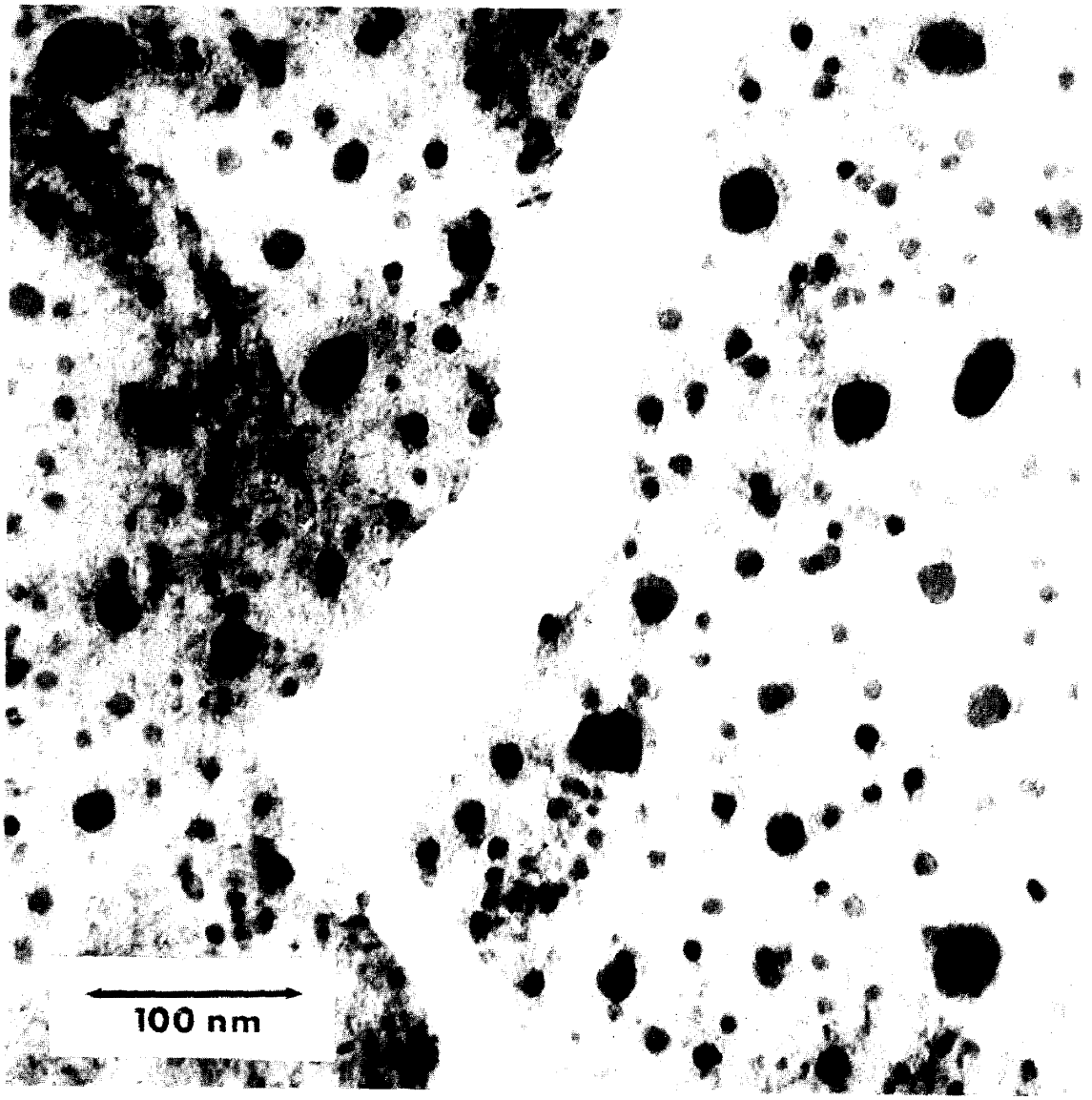

FIG. 5. A 5-nm Fe/TiO_2 specimen following reduction at 773 K for 3 h (see Table 1).

ture and was not previously observed at lower reduction temperatures.

Consistent with previous investigations of Pt/TiO_2 samples reduced at 875 K (*3*, *4*), it is proposed that these low-contrast crystallites are thinner than the high-contrast particles (of similar diameter) observed at lower reduction temperatures (707 K). This would be possible if the three-dimensional particles (present at 707 K) begin to spread over or wet the support surface at 773 K. While these low-contrast particles are thicker than a few monolayers, they are nevertheless believed to be less than or equal to 5.0 nm in height, the original thickness of the iron overlayer. This result was estimated by comparing the contrast differences observed in Fig. 5 with the contrast difference between the iron-containing regions (contiguous film areas) and iron-free areas (light regions adjacent to crystallites) of Fig. 3, as viewed at approxi-

mately the same magnification. It should be noted that the contrast of a given particle is determined by both diffraction and thickness effects (*21*). However, the relative contrast changes observed among a large number of such particles should, except in cases of extreme orientation (epitaxial growth on oriented films or single crystals), be a valid indicator of thickness. For the polycrystalline TiO_2 films used in the present study, the various iron particles are expected to have different orientations with respect to the electron beam. Thus, the low-contrast behavior of many iron particles on different support films and different regions of the same support (e.g., different orientations with respect to the electron beam axis), suggests that this behavior is due primarily to a particle thickness effect.

Reduction at Temperatures of 875 K *or Higher*

Reduction at these higher temperatures brought about additional morphological

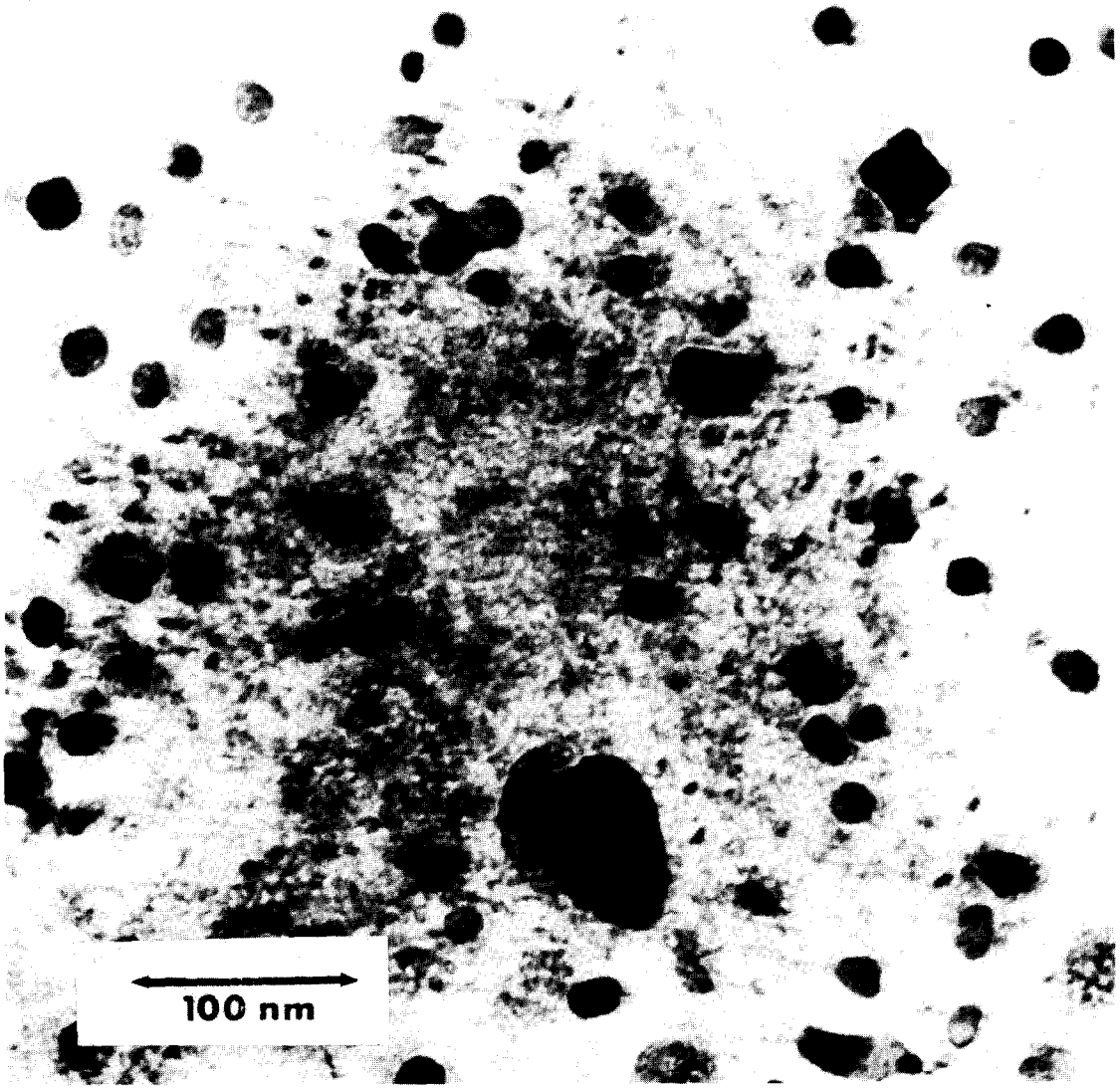

FIG. 6. A 5-nm Fe/TiO_2 specimen following reduction at 875 K for 3 h (see Table 1).

changes in the iron particles. This is shown in Figs. 6 and 7, for reduction at 875 and 928 K, respectively. In particular the sequence of micrographs (Figs. 5, 6, 7) after reduction at 773, 875, and 928 K indicates an increasing tendency for larger particles to assume the "thin-crystal" morphology (or the "pillbox" morphology of Baker *et al.* (*3, 4*)). For example, a relatively large number of crystallites in the range 20–30 nm possess the "thin-crystal" morphology after reduction at 875 K (Fig. 6) while just a few in this size range show this morphology following treatment at 773 K (Fig. 5). In fact, after reduction at 928 K (Fig. 7) there is evidence that much larger crystals (~50 nm) have also adopted this thin-crystal shape.

Particle Size Distributions

To further quantify the reduction behavior described above, particle size distribu-

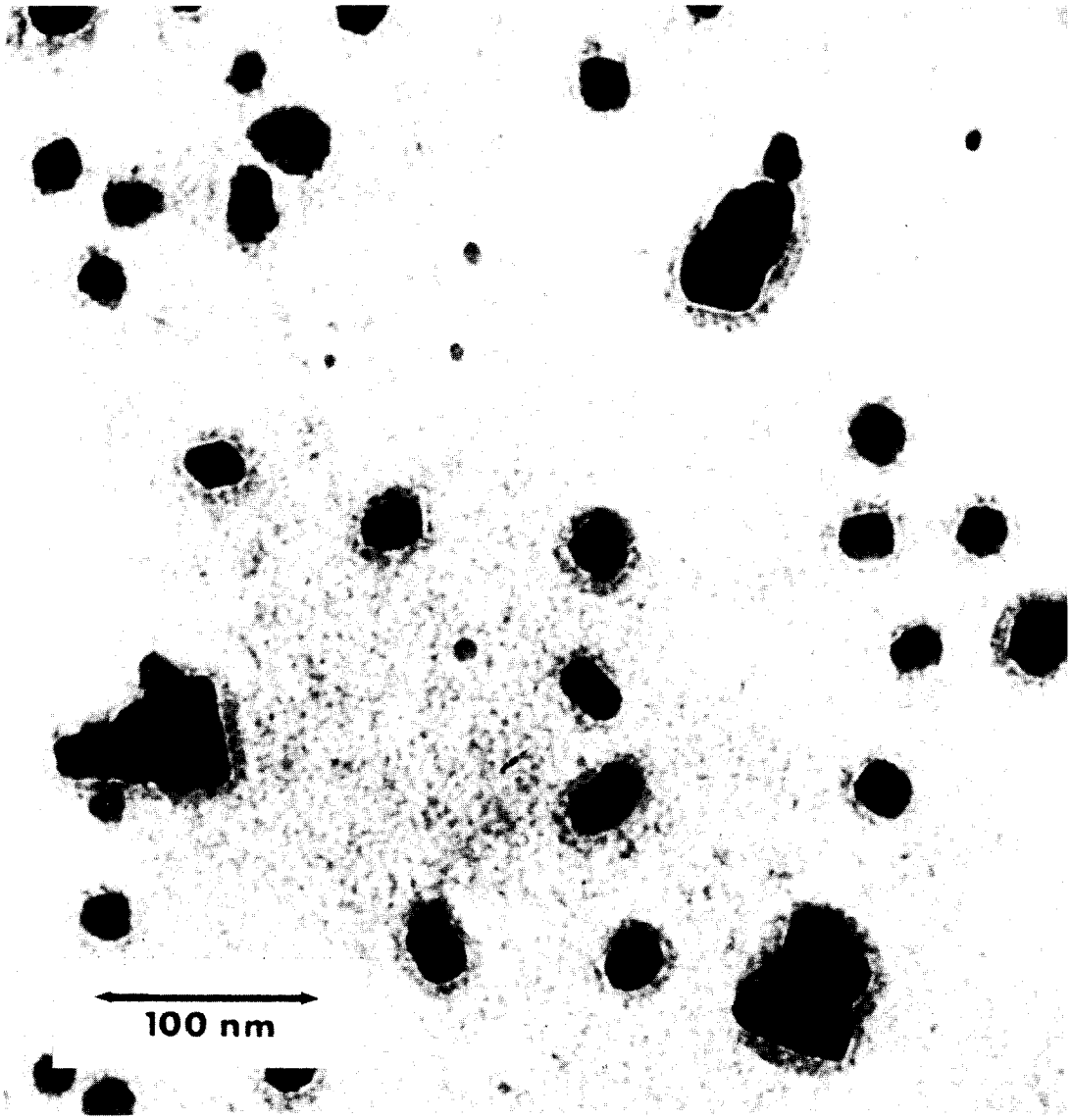

FIG. 7. A 5-nm Fe/TiO_2 specimen following reduction at 928 K for 3 h (see Table 1).

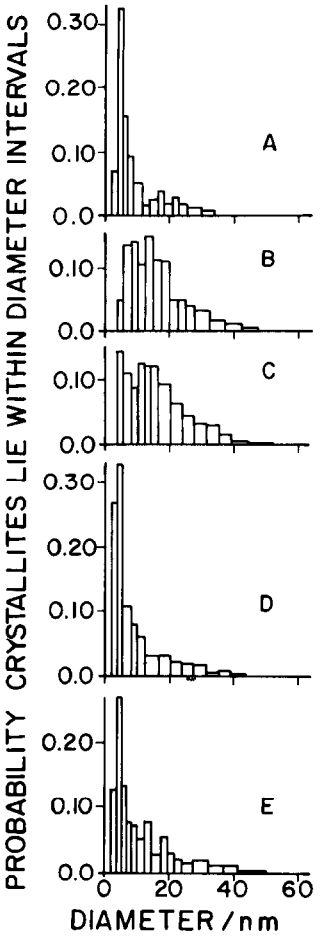

FIG. 8. Particle size distributions for 5-nm Fe/TiO_2 specimens following reduction at the indicated temperatures; (A) 643 K, (B) 707 K, (C) 773 K, (D) 875 K, and (E) 928 K (see Table 1).

tions were determined after the various reduction treatments. These are shown in Fig. 8 for the 5-nm iron overlayer. Similar particle size distributions were obtained for the 3.8-nm iron overlayer, with the only difference being that these distributions were displaced toward smaller particle sizes compared to those for the 5-nm iron overlayer. Each of the distributions in Fig. 8 was obtained by counting approximately 1000 particles. It should also be mentioned that while the particle size intervals used in Fig. 8 are nonuniform in width, the corresponding intensity of each interval has been divided by its width in order that these plots better resemble true probability versus particle size distributions. Finally, for ease in comparison the probability summed over all particle size intervals has been normalized to be the same for each of the particle size distributions.

At the early stages of nucleation (Fig. 8A) the most probable iron crystallite size is approximately 4.5 nm. After continued reduction through 677 to 707 K (Fig. 8B), crystallites with diameters greater than 20 nm are formed at the expense of those with diameters less than 5 nm. Reduction at higher temperatures (Figs. 8C–E), however, results in an apparent "redispersion" of the iron phase. For example, Fig. 8C shows a slight bimodal appearance; and, Figs. 8D and E indicate a strong preference toward smaller diameters, with a large fraction of the crystallites having sizes less than 10 nm. This result is, in fact, not unique to this study, as previous workers (*3*, *4*) studying Pt on TiO_2 saw similar results in this temperature regime.

Of importance for the interpretation of this decrease in iron particle size is the calculation of the "volumetric size distributions." These correspond to plots of the volume of iron that is present (per unit area of titania) within iron particles of a particular particle size interval. Such plots were obtained by multiplying the number of iron particles present (per unit area of titania), in the particle size interval centered at D, by D^3. This corresponds to the assumption that all iron particles are three dimensional. The area, A, under these "volumetric size distributions" then corresponds to the amount of iron present as distinct, three-dimensional particles on the titania support. Comparison of the value of A after progressively higher reduction temperatures shows that A decreases in a monotonic fashion by ca. 30 ± 2% when the temperature is increased from 707 to 928 K. This change in A indicates that reduction of the average particle size is not caused by either atomistic sintering effects or redispersion phenomena but rather from the loss

TABLE 2

TEM Reduction Summary

Reduction temperature (K)	Observed TEM trends	Reduction regimes
Initial iron overlayer	Contiguous Fe film	Low-temperature reduction, nucleation, and growth
608 643	Nonuniform nucleation, most probably particle size $\langle D \rangle < 10$ nm	
677 707	Uniform nucleation, three-dimensional crystallites, $\langle D \rangle > 10$ nm	
773	Contrast between crystallites, $\langle D \rangle \cong 10$ nm	Spreading of iron over support
875 973	Contrast between crystallites, decrease in number density and volume of crystallites, $\langle D \rangle \leq 10$ nm	Diffuse spreading of iron over support or diffusion of iron into support

of observable or highly contrasted material. Furthermore, reference to Figs. 4 through 7 shows that the assumption of constant, three-dimensional particle morphology is not correct, since the crystallites become thinner after reductions at higher temperatures. Thus, the decrease in the amount of "observable iron" at higher temperatures is actually more pronounced than the decrease in A would suggest. (For example, if cubic iron particles are converted into semispherical particles during hydrogen treatment at 928 K, then the observed decrease in A corresponds to a 50% decrease in the amount of observable iron.) This loss of iron must reflect a conversion of iron from three-dimensional crystallites into another form not observed by TEM. The formation of new, three-dimensional crystallites below the TEM focal plane of the titania surface was ruled out by focusing experiments. Instead, possible mechanisms that would account for this behavior include a diffuse spreading of iron *over* the support or a diffusion of iron *into* the support.

SUMMARY/CONCLUSIONS

The reduction behavior of iron supported on titania can be divided into three distinct regimes, as summarized in Table 2. Reduction at temperatures less than or equal to 707 K (see Figs. 3, 4, and 8A and B) leads to changes in the morphology of iron that can be explained in terms of nucleation and growth processes. At temperatures of 773 K (see Figs. 5 and 8C) smaller crystallites are observed to spread over or wet the support surface, becoming light in appearance, as they adopt a "thin-crystal morphology." Finally, reduction at temperatures of 875 K or higher causes large iron particles to adopt this "thin-crystal morphology" (Figs. 6 and 7) and the average iron particle size is observed to decrease (Figs. 8D and E). These changes are accompanied by a decrease in the amount of iron present as distinct crystallites on the support. This is attributed to a diffuse spreading of iron *over* the support or a diffusion of iron *into* the support. Distinction between these two processes is not

possible using TEM along. In Part II of this series, however, XPS and CEMS will be used to study further these phenomena. It will be shown that this loss of iron from distinct crystallites upon high-temperature reduction is due primarily to the diffusion of iron into the support.

ACKNOWLEDGMENTS

See the acknowledgments of Part III.

REFERENCES

1. Tauster, S. J., Fung, S. C., and Garten, R. L., *J. Amer. Chem. Soc.* **100,** 170 (1978).
2. Tauster, S. J., and Fung, S. C., *J. Catal.* **55,** 29 (1978).
3. Baker, R. T. K., Prestridge, E. B., and Garten, R. L., *J. Catal.* **56,** 390 (1979).
4. Baker, R. T. K., Prestridge, E. B., and Garten, R. L., *J. Catal.* **59,** 293 (1979).
5. Vannice, M. A., and Garten, R. L., *J. Catal.* **56,** 236 (1979).
6. Vannice, M. A., and Garten, R. L., *J. Catal.* **63,** 255 (1980).
7. Gajardo, P., Gleason, E. F., Katzer, J. R., and Sleight, A. W., *in* "Proceedings, 7th International Congress on Catalysis, Tokyo, 1980," Paper No. E1.
8. Meriaudeau, P., Ellestad, H., and Naccache, C., *in* "Proceedings, 7th International Congress on Catalysis, Tokyo, 1980," Paper No. E2.
9. Dickson, J. G., Katz, L., and Ward, R., *J. Amer. Chem. Soc.* **83,** 3026 (1961).
10. Horsley, J. A., *J. Amer. Chem. Soc.* **101,** 2870 (1979).
11. Goodenough, J. B., *in* "Progress in Solid State Chemistry," Vol. 5 (H. Reiss, Ed.). Pergamon, New York, 1971.
12. Hass, G., *Vacuum* **2,** 331 (1952).
13. Hickman, J. W., and Gulbransen, E. A., *Anal. Chem.* **20,** 158 (1948).
14. Hansen, M., "Constitution of Binary Alloys." McGraw-Hill, New York, 1958.
15. Tatarchuk, B. J., Chludzinski, J. J., Sherwood, R. D., Dumesic, J. A., and Baker, R. T. K., *J. Catal.* **70,** 433 (1981).
16. Shannon, R. D., *J. Appl. Physics* **35,** 3414 (1964).
17. Kingsbury, P. I., Ohlsen, W. D., and Johnson, O. W., *Phys. Rev.* **175,** 1091 (1968).
18. Johnson, O. W., Ohlsen, W. D., and Kingsbury, P. I., *Phys. Rev.* **175,** 1102 (1968).
19. Iyengar, R. D., and Codell, M., *Advan. Colloid Interface Sci.* **3,** 365 (1972).
20. Iyengar, R. D., Codell, M., Gisser, H., and Weisberg, J., *Phys. Chem. Nene Folge* **89,** 325 (1974).
21. Treacy, M. M. J., and Howie, A. J., *J. Catal.* **63,** 265 (1980).